Available online at www.sciencedirect.com

ScienceDirect

Ceramics International 40 (2014) 859–869

CERAMICS INTERNATIONAL

www.elsevier.com/locate/ceramint

Utility of by-product quantum dots obtained during synthesis of Cu_2ZnSnS_4 colloidal ink

Prashant K. Sarswat*[,1], Michael L. Free

Department of Metallurgical Engineering, University of Utah, Salt Lake City, UTAH 84112, United States

Received 25 May 2013; received in revised form 20 June 2013; accepted 22 June 2013
Available online 3 July 2013

Abstract

This manuscript discusses the utilization and evaluation of kesterite modified multicolor quantum dots (QDs) obtained as a by-product during synthesis of photovoltaic kesterite material. It was observed that luminescence and optical properties of these nanocrystals highly depends on many factors such as type of solvent, sulfur source, the concentration of percursors, intercapping ligands and reaction temperature. The investigation indicates that these QDs contain defect levels of copper and tin, that are believed to be responsible for green color luminescence. These QDs are highly stable and maintain their resistance against photodegradation. The maximum quantum yield of these QDs was ~0.32 and it remains stable for many days. Raman analysis, X-ray photoelectron spectroscopy, and FTIR spectroscopy suggest that most of these QDs contain ZnS and some ZnO due to chemisorbed oxygen. A light emitting diode was fabricated using a solid host containing these QDs.

Keywords: Nanocrystals; By-product; Kesterite; Light emitting diode

1. Introduction

In recent years colloidal semiconducting nanocrystals or quantum dots (QDs) have emerged as frontier materials for utility in high efficiency devices, white light source (such as light emitting diode or LED), display devices, optical sensors, and other applications in nanoscience and biotechnology [1]. Amongst them cadmium free chalcogenide type quantum dots are of considerable importance because of their utility as non-toxic, enviromentally friendly precursors as well as their uses in applications such as biolabeling and forster resonance energy transfer [1]. One methodology for LED fabrication is direct production of photons by electroluminscence, whereas a popular alternative methodology to obtain multicolor LEDs is to apply a thin coating of phosphor material such as, $Y_3Al_5O_{12}$:Ce (Ce:YAG) (although some of the emission from the host LED remains unconverted) over the primary light source [2]. Using this approach, one can fabricate LEDs which appear white. For green light emitting diodes, considerable intensity and quantum efficiency have been achieved for many phosphors such as $Ca_2Al_3O_6F:Eu^{2+}$, Eu^{2+}-doped $Ba_3Si_6O_{12}N_2$, β-SiAlON:Eu^{2+}, and $Ba_2Gd_2Si_4O_{13}:Ce^{3+},Tb^{3+}$ [3–6]. For white light emitting diodes YAG:Ce is frequently used as phosphor [3]. It is important to note that most of these solid state lighting phosphors utilize rare earth metals, which are very costly and have limited availability. Recently, copper indium selenide (CIS) type quantum dots have been utilized for solid state white lighting [7,8]. It has been reported that high- flouroscence CIS type QDs with color tunable optical properties, can be synthsized using a wet synthesis approach [7,8]. In addition, the emission quantum yield of CIS quantum dots can be increased by synthesizing a QD-core shell structure [7,8]. It was also reported that there is an energy loss due to light scattering caused by micrometer sized phosphor particles [7,8]. Hence, there is a need to expedite research for nanoparticles of size less than 10 nm, which can be an alternative to conventional rare earth metals containing large particles for flouroscence applications. Another interest in colloidal quantum dots is their utility as quantum dots solids [9]. Nanocrystalline solids can be synthesized from nanocrystal suspensions. The most practiced technique is drop casting. A suspension of quantum dots is applied to a desired substrate and evaporation follows. Based on

*Corresponding author. Tel.: +1 801 520 6919.
E-mail address: saraswatp@gmail.com (P.K. Sarswat).
[1]Address: 135S, 1460 E, Room 412, Salt Lake city, UT 84112.

0272-8842/$ - see front matter © 2013 Elsevier Ltd and Techna Group S.r.l. All rights reserved.
http://dx.doi.org/10.1016/j.ceramint.2013.06.080

the nature of solvent one can synthesize a one-dimensional or two-dimensional assembly of crystals. Fast evaporation of solvent generally results in amorphous solids. However, slow evaporation often leads to a high quality superlattice. Recently, copper zinc tin sulfide type nanocrystals were studied and quantum confinement phenomenon exhibited by them was reported [10,11]. Colloidal nanocrystals of size 2–7 mm was reported, and absorbance spectra of these nanocrystals were a function of size as expected. These observations suggest that there is a scope of size reduction and potential as an optical device for kesterite modified nanocrystal. In view of these research needs, a detailed investigation was carried out by adjusting semiconducting crystal dimension in order to achieve subsequent changes in optical properties.

2. Experiments

2.1. Synthesis of kesterite modified nanocrystals

To obtain monodisperse QDs, it is very essential to control nucleation and growth steps. This can be achieved by quick addition of precursors and vigorous stirring of coordinating solvent (in our case elemental sulfur dissolved in olyelamine) in a reaction flask at elevated temperature, so that concentration increase above the critical concentration required for nucleation. A rapid decrease in concentration of precursor decelerates and subsequently stops nucleation. Good control over reaction temperature and quenching is also very important in order to produce the desired particle size [1]. If monomer concentration is below the nucleation threshold (but also above the saturation level), small crystal growth is fast. However, low concentrations result in Ostwald ripening. In a typical experiment (except sample 1 where a high zinc stearate concentration ~5 times that of CuI was used) CuI (0.28 mmol), zinc accetate (or zinc stearate) (0.15 mmol), tin accetate (0.15 mmol), and thiourea (0.65 mmol) were loaded in a 3-neck flask containing 1 ocatadecene~10 ml and 3–4 ml oleylamine. It was marked as sample 2. An inert atmosphere was maintained prior to reaction and continued till the end of reaction using an uninterrupted supply of argon. Prior to argon back filling, the flask was degassed several times.

For quantum dot growth, the flask was heated up to 100 °C during degassing and backfilling and further heated up to a temperature of ~290 °C. This temperature was maintained for different time periods ~10, 20, 30, and 45 min. After reaction, the suspension was repeatedly cleaned and washed with ethanol–isopropanol or ethanol–hexane–isopropanol. Large sized black-brown crystals (ink) were separated from the rest of the supernatant using gravity separation. This supernatant (sample 3) was investigated in detail. For sample 4 (supernatant), hydrated copper chloride, hydrated zinc chloride, tin chloride, and thiourea were used for synthesis. The molar concentration of precursors was very similar to that with sample 2. Experiments were also performed in open air environment to evaluate the effect of oxygen. These samples were not investigated in detail as most of the focus was to investigate $Cu_aZn_bSn_cS_d$ type nanocrystals. However some of the characterization results are presented in the manuscript. Fig. 1 shows images of UV illuminated samples. Sample 5 preparation protocol is similar to sample 3, except nanocrystals (from supernatant) were redispersed in chloroform.

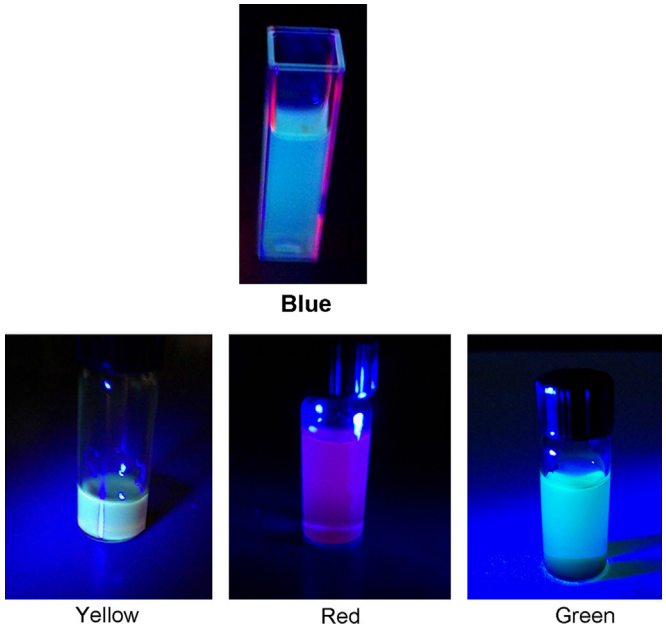

Fig. 1. Four different color emitting quantum dots synthesized using environmentally friendly precursors. (For interpretation of the references to color in this figure legend, the reader is referred to the web version of this article.)

2.2. Synthesis of luminescence epoxy resin for light emitting diode

After synthesis of luminescent QDs, incorporation of these nanocrystals into variety of transparent sols or solid hosts is challenging. We have utilized Buhler epoxy resin and hardener for this purpose. For primary investigation, Buehler Epothin epoxy resin was mixed with our $CHCl_3$-quantum dot colloidal dispersion. Volatile components were removed by slowly heating at a temperature of ~50° C. Two different layers were observed after slow heating. A distinct boundary was observed while irradiating this sample with UV light. A portion of resin-QD mixture was removed and epothin hardener was mixed into it (ratio ~5:2). Some of this mixture was utilized for green-white LED fabrication and some mixture was left in the beaker for 24 h. UV light LED (specification: wavelength = 400 nm, luminous intensity: 12 mW typ. @ 20 mA, power dissipation: 120 mW) was utilized as the primary source of light. Other details regarding investigation of these LED will be discussed in results and discussion section.

2.3. Characterizations

The phase characterization of colloidal nanocrystals was performed using an R 3000 QE Raman spectrophotometer. The Wavelength of laser excitation for Raman measurements was 785 nm and the laser power was ~100 mW. The nanocrystal size

and morphology were studied using an FEI 200 KeV Tecnai G2 F20 Transmission electron microscope. A droplet of solution containing QDs (hexane or chloroform) was cast on a TEM grid, which was further evacuated and dried. UV–Visible absorption spectra were recorded using an Ocean Optics spectrophotometer equipped with OOI Base 32 software. These optical characterizations were done using dispersed samples properly kept in a quartz cell. X-ray photoelectron spectroscopy (XPS) experiments were carried out using the monochromatic AlK_{α} source equipped Kratos Axis Ultra DLD instrument. The spot size was ~400 μm. Dwell time was ~200 ms, and step size was kept ~1 eV. FTIR spectroscopy was carried out using a PerkinElmer Frontier™ FTIR spectrophotometer equipped with an ATR accessory and Spectrum 10™ software suite.

3. Results and discussions

3.1. Raman spectroscopy

Fig. 2 shows Raman spectra of large sized nanocrystals (from sample 2) collected from the lower portion of the synthesis cell, after gravity separation. This spectrum suggests that colloidal ink contains CZTS, as most of the peak position is consistent with earlier reported Raman spectra [10–14]. It also can be observed that Raman peaks for the sample, synthesized for a duration of ~45 min are intense compared to that synthesized for ~15–20 min. Fig. 3 shows Raman spectra of the quantum dots (samples collected from supernatant), recorded in back scattering mode. In most of the cases analyses were conducted for the samples synthesized for 45 min duration. The peak positions of these spectra were compared with the Raman peaks of CZTS, ZnS, ZnO, copper tin sulfide, $Cu_{2-x}S$, and SnS_2. Sample 1 (Fig. 3 (a)) shows peaks or shoulders at ~625, 654, and 677 cm^{-1}. These peaks can be assigned to 2TO (transverse optical) overtone, combination of TO and LO (longitudinal optical) mode, and 2 LO overtone of ZnS crystals [15–17]. Sample 5 (Fig. 3(b, c)), showing green luminescence, shows distinct intense peaks or shoulders at ~458, 622, 647, and 671 cm^{-1}. These peaks or shoulders also match with Raman peaks corresponding to [LO+TA (transverse acoustic)]x mode, 2TO overtone, combination of TO and LO mode, and 2 LO overtone of ZnS crystals, respectively [15–17]. Sample 3 also shows very similar peaks. Colloidal nanocrystals showing yellow luminescence, (Fig. 3 (d)) exhibit strong peaks at ~377 cm^{-1}, which corresponds to the A_1(TO) Raman mode of ZnO nanostructure [18]. This observation indicates formation of ZnO due to synthesis in open air environment. Sample 4 (blue luminescence) shows strong Raman peaks at ~369 and 337 cm^{-1} that correspond to SO (surface optical) and LO Raman mode of ZnS crystal (see Fig. 3(e)). Peaks are also obtained at ~622, 647, and 677 cm^{-1}, (see Fig. 3 (F)) which correspond to 2TO overtone, combination of TO and LO mode, and 2 LO overtone of ZnS nanocrystals [15–17]. It was also observed that some of the Raman peaks were shifted from the peaks of pure ZnS nanocrystals. This shift can be attributed to strain effect, nature of substrate, type of dopants, and discontinuity in lattice due to dopants. Overall, this analysis suggests that nanocrystals from this study contain ZnS (when synthesized in inert atmosphere) and ZnO (when synthesis was carried out in air), which may responsible for luminescence behavior.

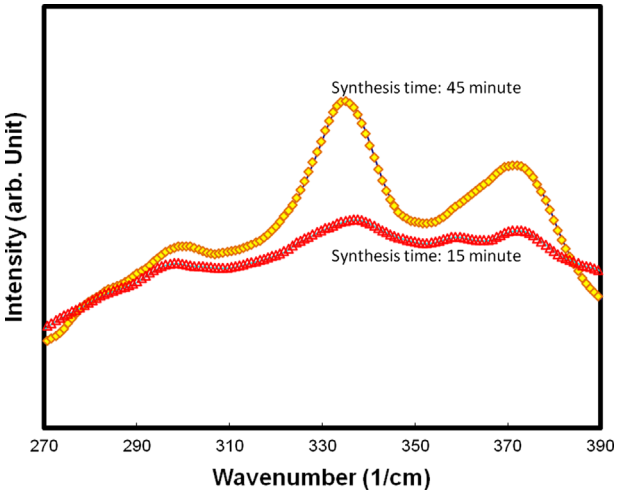

Fig. 2. Raman spectrum of large sized nanocrystals.

3.2. Solubility/Dispersibility

Solubility (or dispersibility) of as-synthesized quantum dots was examined in various solvents. It was observed that these quantum dots are soluble in most of the organic solvents such as acetone, ethanol and isopropanol. However, these as synthesized quantum dots are not water soluble. Fig. 4 shows such an image of quantum dots in water.

3.3. UV–vis spectroscopy

Fig. 5 shows absorbance spectra of $Cu_aZn_bSn_cS_d$ type quantum dots with different values of a, b, c, and d. The details of stoichiometric ratios (a, b, c, and d) are listed on Table 1. The absorbance approaches zero at energy levels of 2.6 eV, 2.94 eV, and 3.10 eV for QDs of sample 1, sample 3, and sample 4 respectively. The absorbance in these colloidal nanocrystals depends on many factors such as energy of incoming photons, density of vacant states in the conduction band as well as the density of electrons in the valance band [1]. From normalized UV absorption spectra, it has been found that peak position varies from 300 to 336 nm, which corresponds to (E_g=4.10 and 3.68 eV). It is very obvious from absorbance spectra that QDs from this study show a blue shift compared to bulk sphalerite (absorbance maximum was reported at ~340 nm). This blue shift indicates a reduction in particle size [1]. The band gap energy for CuS QDs was reported to be ~2.35 eV, which is higher than bulk CuS [19]. In this study no distinct band at ~525 nm was observed, thus CuS QDs are not present in significant quantity. We have utilized the Brus equation to evaluate the particle size-band edge relationship [20]:

$$E_g(QDs) = E_g(bulk) + \left(\frac{h^2}{8R^2}\right)\left(\frac{m_h + m_e}{m_h m_e}\right) - \frac{1.8e^2}{4\pi\varepsilon_o\varepsilon_r R} \quad (1)$$

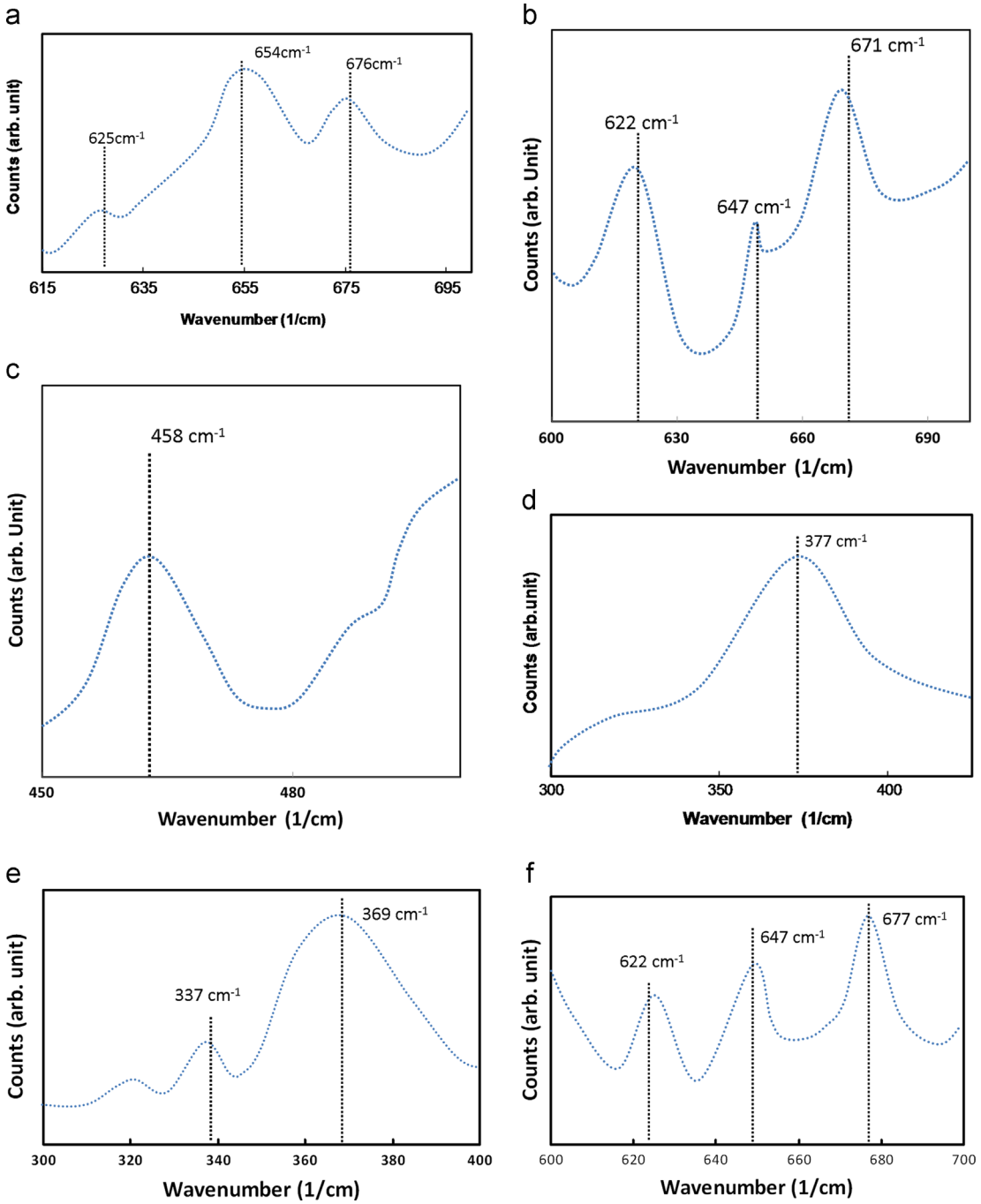

Fig. 3. Raman spectroscopy of multi-colored QDs: (a) Red color (sample 1) exhibiting 2TO (transverse optical) overtone, combination of TO and LO (longitudinal optical) mode, and 2 LO overtone. (b) Green color (sample 5), showing [LO+ TA (transverse acoustic)]x mode, (c) Green color (sample 5) showing 2TO overtone, combination of TO and LO mode, and 2 LO overtone (d) Yellow color (synthesized in O_2 presence), showing A_1(TO) Raman mode of ZnO (e) Sample 4 showing SO and LO Raman mode, and (f) Sample 4 showing 2TO overtone, combination of TO and LO mode, and 2 LO overtone. (For interpretation of the references to color in this figure legend, the reader is referred to the web version of this article.)

where m_h and m_e are effective hole and electron mass respectively, R is the radius of quantum dot, h is the Plank constant, e is the electronic charge, E_g is the band gap energy ε_r was chosen to be ~7, and ε_0 is permittivity of free space.

Using Eq. (1), the radius versus 'difference in band gap' (for bulk and nanosized crystals) was plotted using different values of effective mass in Fig. 6. For stoichiometric CZTS the electron effective mass was reported ~0.18 m, whereas the hole effective mass is strongly anisotropic [21]. It can be seen that the band representing the E_g-radius relationship for low values of electron effective mass (such as CZTS), is above that for relatively high values of electron effective mass (such as ZnS). Further, for CZTSe this curve will be expected to be above all of these curves, due to the relatively small effective electron mass. Careful observation of these curves suggests that for the low effective mass regime a size change (which corresponds to equal

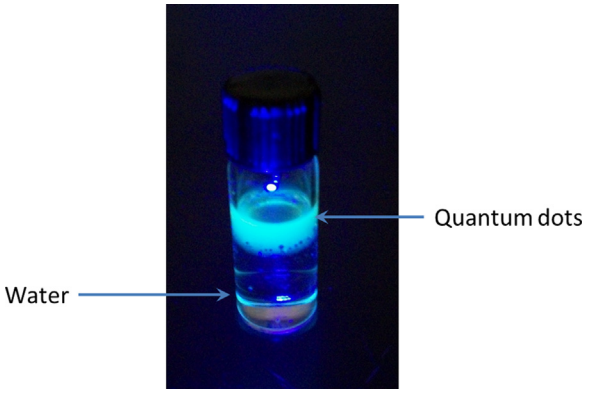

Fig. 4. Quantum dots containing liquid and water.

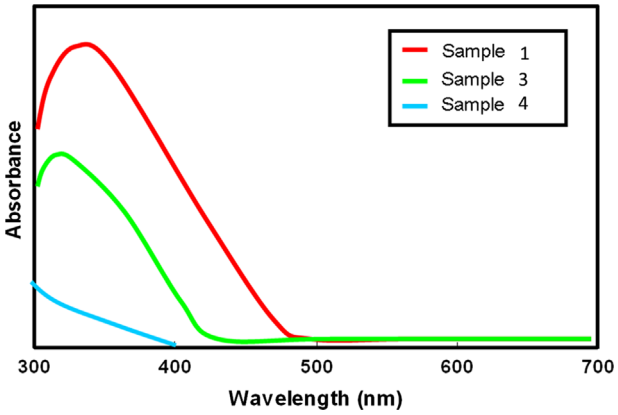

Fig. 5. Absorbance spectra of different QDs.

Table 1
Atomic percentage of various elements in QDs.

Sample ID	Luminescence	Cu	Zn	Sn	S
1	Red	–	0.39	–	2.40
2	–	0.25	0.16	0.12	0.87
3	Green	0.07	0.55	0.06	0.55
4	Blue	–	1.30	0.32	0.84
5	Green	0.10	1.17	0.07	1.78

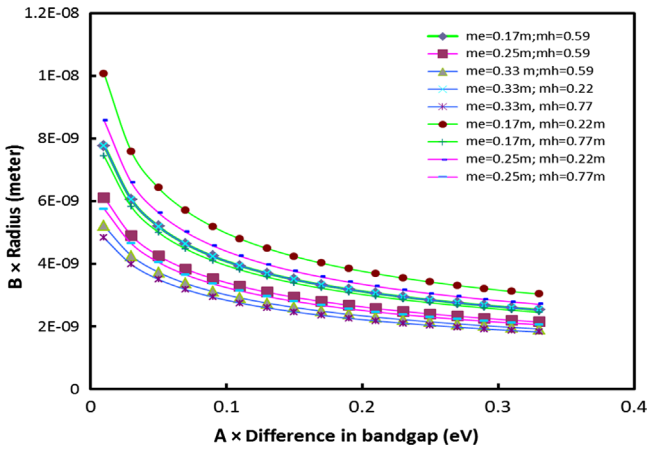

Fig. 6. Difference in band gap-size relationship for different effective mass. A and B are suitable multipliers.

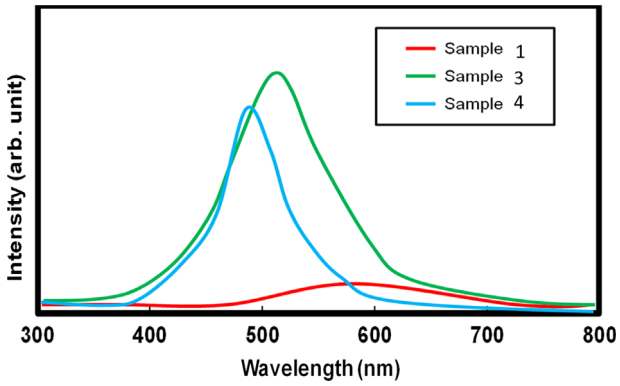

Fig. 7. Emission spectra of different QDs.

shift in absorbance peak) was twice as high compared to that for high effective mass. The excitonic Bohr radius for ZnS nanocrystal is ~2.2–2.7 nm [22]. For the bulk copper sulfide, the band gap varies from ~1.2 to 2.0 eV [19]. The calculated excitonic Bohr radius for copper sulfide was ~3–5 nm, which was obtained by dividing the dielectric constant by the reduced mass [19]. For CZTS, the excitonic Bohr radius was estimated to be ~2.5 to 3.3 nm [10]. Hence, it can be said that most of these crystalline phases showing quantum confinement have a radius of ~2–3 nm. Fig. 6 shows that quantum confinement for large sized particles, which is directly related to excitonic Bohr radius (which is similar for the phases discussed), can be experienced as a small change in band gap shift. On the other hand, for smaller sized crystals it will be evidenced in the form of a large difference in band gap. Hence, assessment based on the Brus equation and absorbance data strengthen the fact that ZnS is more prone to quantum confinement than CuS or CZTS. For smaller blue shift (for red QDs), which can be observed from the graph, size of particle is large, whereas for larger blue shift (green and blue QDs) particle size is smaller as evidenced in TEM images. A well-known fact is that enhanced orbital overlapping of dopants with host atoms (partially due to quantum confinement) supports enhanced luminescence efficiency caused by guest-host energy transfer [23]. In our case these facts were corroborated by XPS results and emission spectra.

Absorbance bands at positions in the range ~300–336 nm and their peak FWHM suggests a dispersed size distribution. From photoluminescence spectra (Fig. 7), it was observed that the intensity of green light was highest, whereas quantum dots emitting red color had minimum intensity. It was also observed that sample showing red luminescence has low copper and moderate zinc concentrations, whereas the blue color emitting sample shows high zinc as well as tin with low copper. Samples emitting green luminescence show the presence of

copper along with tin. This observation suggests that induced levels arise due to doping of foreign elements like copper. It was reported that green luminescence (wavelength range ~495–570 nm) in copper doped zinc sulfide QDs is due to the copper induced level [24]. An emission band centered at ~480 nm is believed due to such level. In this study a green emission band was centered at ~510 nm, and is not very distant from the reported value [24]. Hence, it is very clear that there are some additional levels (the undoped ZnS emission band was centered at ~424 nm). For tin sulfide QDs, peaks were observed at ~545 and 490 nm [25]; other peaks were not observed, very close to such locations. Sample 4 which shows blue luminescence, is possibly due to re-dispersion of OA-QDs conjugates in aqueous phase [20]. In all cases an excitation wavelength of ~400 nm was used. Based on ISO standards this wavelength is commonly known as ultraviolet A (UVA). It was observed that nanocrystals reacted less than 30 min did not show an obvious emission peak. It is possible that this is due to the absence of a crystallized phase and the presence of amorphous solids. After detailed comparison it was concluded that such green emission is almost solvent independent. Hence effects due to superposition of spectra were neglected. These emission peaks exhibit energy smaller than the band gap energy, which generally suggests radiative recombination of excitons.

The most accepted principle for formation of these quantum dots is that: metal ions attached to polymeric chains react with sulfur to form a cluster of primary, secondary, or tertiary sulfide. These sulfides finally get consumed and subsequently form the final product. It was observed that the fluorescence intensity of QDs was negligible during the beginning of experiments. The intensity increases during the course of experiments and reaches a maximum value. After this maximum it starts decreasing at a steady rate. This assessment suggests that during the primary stage of synthesis, the total area of nanocrystal surface increases because of nucleation and growth [1].

3.4. Quantum yield

Highest quantum yield of our QDs was ~0.32 for sample 3. However, for sample 4, the quantum yield was ~0.23 and less than ~0.10 for sample 1. Quantum yield was determined using standard protocol [26].

3.5. Evidence of electronic coupling

In many cases electronic coupling between quantum dots occurs and it is very similar to closed packed solid arrays of QDs. It was also observed that the strength of electronic couplings depends on QDs size and interparticle distance. The strength of electronic coupling generally decreases when interdot distance increases [1]. At large distance most of the QDs maintain their phase integrity as well as an isolated electronic structure, and hence these arrays behave as an insulator. To ensure electronic coupling, a difference in absorbance spectra of colloidal QDs and QD-Solid in transparent substrate was examined. An inter-quantum dot coupling was observed due to extension of an electron/hole wave function outside of the quantum dot boundary. This phenomenon was observed in the form of the red shift in optical spectra. In our case almost all QD solid exhibited a red shift, though this value was not very high ~12 nm. This red shift was highest for green color and lowest for red color quantum dots.

Intercrystal distance can be modified by the ligand exchange process. Oleylamine use leads to an interdot distance ~18 Å, in contrast use of ethanediamine (EDA) and hexylamine, which are relatively small molecules, are likely to lead to shorter interdot distances [27]. Hence, it will be interesting to observe the effects of such legend exchange process on optical performance of these nanocrystals. These experiments are in progress.

3.6. XPS analysis

To obtain more insights about electronic states and binding energy of our QDs, XPS analysis was carried out (See Figs. 8a, b). Based on XPS results, it was reported that pure copper sulfide shows peaks at ~939.32 eV and at ~342.4 eV [28,29]. Sample 1 (showing red luminescence and high amount of zinc) shows peak at 936 eV, which is ~3.0 eV chemically shifted from the peak of CuS [28,29]. It indicates the presence of copper ion in ZnS. Zn 2p3/2 line standard location is ~1021.7 eV and Zn 2p1/2 line is located at ~1044.70. These lines are observed for most of our samples. No evidence of CuO or CuS at ~952.4 eV was observed. Cu 2p3/2 was reported at ~931–933 eV. For CuO, the 2p3/2 location is ~933.5 eV. No such peaks at these locations were observed. S 2p has variable locations ~160–164 eV [28,29]. Sample 4 contains almost no copper, although the Zn: Sn ratio was 1.30:0.32. It was observed that this sample was sulfur deficient. For Sample 3, Cu: Zn: Sn: S ratio was: 0.07: 0.55: 0.06: 0.56. It is believed that green luminescence for this sample is characteristic of transition from defect level to an induced 't2' level (caused by copper) [24]. The ratio of Zn:S in this case was ~1:1. For sample 3 Zn 2p peaks were observed at 1044 and 1021 eV, which were separated with an energy of ~23 eV. Such peak separation is consistent with standard separation of ~22.97 eV for the zinc (II) oxidation state. This sample contains a peak at 498 eV, which indicates ZnO in nanocrystals [30]. For sample 4, tin 3d5/2 peaks were observed at 487 and 495 eV, which were separated with 8 eV. Zn 2p peaks were observed at 1045 and 1022.1 eV, which were separated with an energy of ~23 eV, suggesting Zn (II) oxidation state. No distinct peak corresponding to Cu was observed in this case. An O1S peak was obtained centered on 529 eV in many of our samples. In most cases this peak contains more than one component and a Shirley background. Zn–O bonding corresponds to peak at 528.5 eV, while peaks at 530 and 531 correspond to (OH/O_2^-) and H_2O respectively. Sample 5 and sample 3 were prepared using very similar conditions, and they show a peak at ~530.0 eV, whereas CZTS large crystals, dissolved in toluene, show a peak at

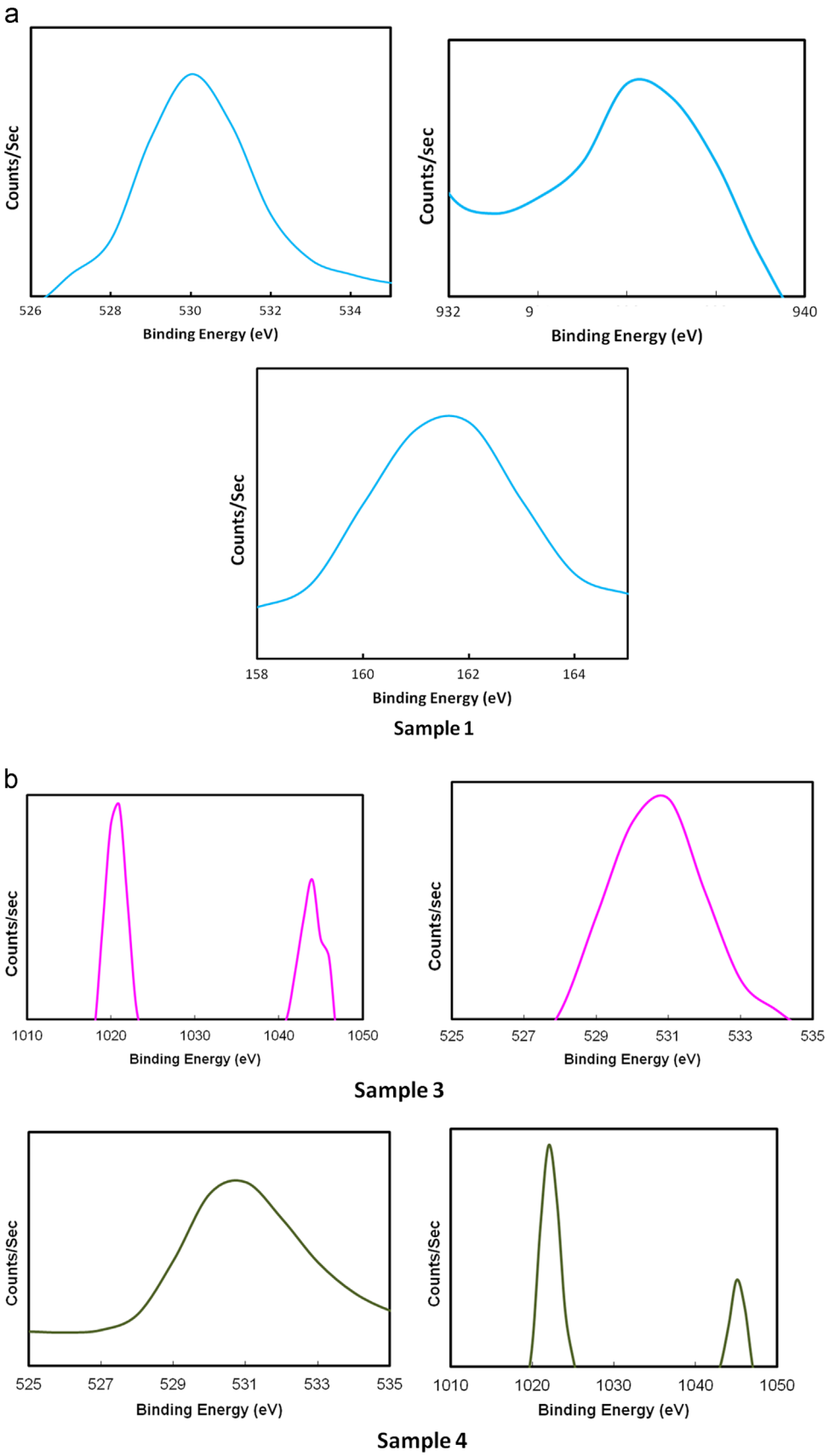

Fig. 8. (a), (b): X-ray photoelectron spectroscopy of samples.

531.5 eV. This peak is close to O1(s(b)). This information suggests the presence of some water vapor component in large sized CZTS crystals as well as different traces of defective and/or extraneous components. Hence, the presence of chemisorbed oxygen and secondary phases such as Zn_xO_y cannot be ruled out. It is interesting to note that for samples 4 (relatively high concentration of tin as revealed by elemental characterizations), O1S peaks were found to be shifted towards higher binding energy. It was reported that for Sn, SnO and SnO_2, the binding energy of Sn 3d5/2 peak was 485, 486.8, and 487.16 eV. Asymmetry indicates the presence of multivalency in these cases. Samples 3 exhibited peak at 48 V, whereas other samples show peaks towards the higher binding energy side. Sample 4 in particular, shows a peak at 487 eV. Hence, this analysis suggests that QDs showing green color contain copper doped ZnS with partial presence of chemisorbed oxygen. Results also suggest the presence of tin as well as the absence of copper oxide or sulfide in these QDs.

3.7. FTIR spectroscopy

FTIR spectra (See Fig. 9a) show a distinct peak at 910 cm^{-1} (Sample 1: red), and 965 cm^{-1} (sample 3: green nanocrystal) which can be assigned to NH_2 bending [31,32]. NH_2 scissor mode is not evident as there is an absence of a peak at ~1568 cm^{-1} [31,32]. A peak at 720 cm^{-1} for sample 1 also likely represents CH_2 bending and some out of phase rocking mode. Sample 1 shows a peak at ~1712 cm^{-1} corresponding to –C=O stretch, possibly due to traces of residual acetate or stearate. The spectrum corresponding to sample 4 (blue color) shows a peak at ~1041 cm^{-1}, which is due to C–N stretching [31,32]. This spectrum also shows a peak at ~1684 cm^{-1}, which is close to the –C=O stretch of amide group and stretching of –C=C–group [31,32]. This sample also shows a peak at ~2890 cm^{-1}, which is an indication of the weak appearance of a methine unit. The presence of the –C–O alcohol unit is also evidenced by the peak observed at ~1091 cm^{-1} [31,32]. A peak at ~1466 cm^{-1} (for sample 3) is due to –C–H bending, whereas peaks at 2851 and 2921 cm^{-1} are associated with C-H stretching. A peak at 1302 cm^{-1} corresponds to –C–O stretch [31,32]. A deepening in these peaks was observed when there is an increase of carbon atoms (red). These observations also suggest that most of the QDs are surrounded by linker molecules. In most cases the linker molecule is oleylamine. Ligand exchange experiments were also conducted by dispersing and stirring sample 3 for 24 h into other organic solvents such as dodecanethiol containing a thiol group. FTIR spectra show disappearance of a peak at ~3400 cm^{-1} (See Fig. 9b) due to amine stretching when a ligand exchange was done using dodecanethiol. It suggests that most of the capping oleylamine was removed. One of the advantages of the thiol group is its binding ability to the surface and anchoring for other organic molecules such as proteins. This enables utility of quantum dots in multiple applications including bioimaging, biosensing, and molecular diagnostics of various diseases. It was observed that quantum yield of our QDs diminishes (up to 50% reduction) after ligand exchange. Many other alternatives such as QDs funtionalization with mercaptoacetic acid or mercaptosuccinic acids were reported for quantum yield improvement [33]. Theoretical studies suggest that thiolic hydrogen should be removed in order to achieve strong binding between ZnS and thiols [33]. Such techniques can be applied for quantum yield enhancement. These experiments are in progress.

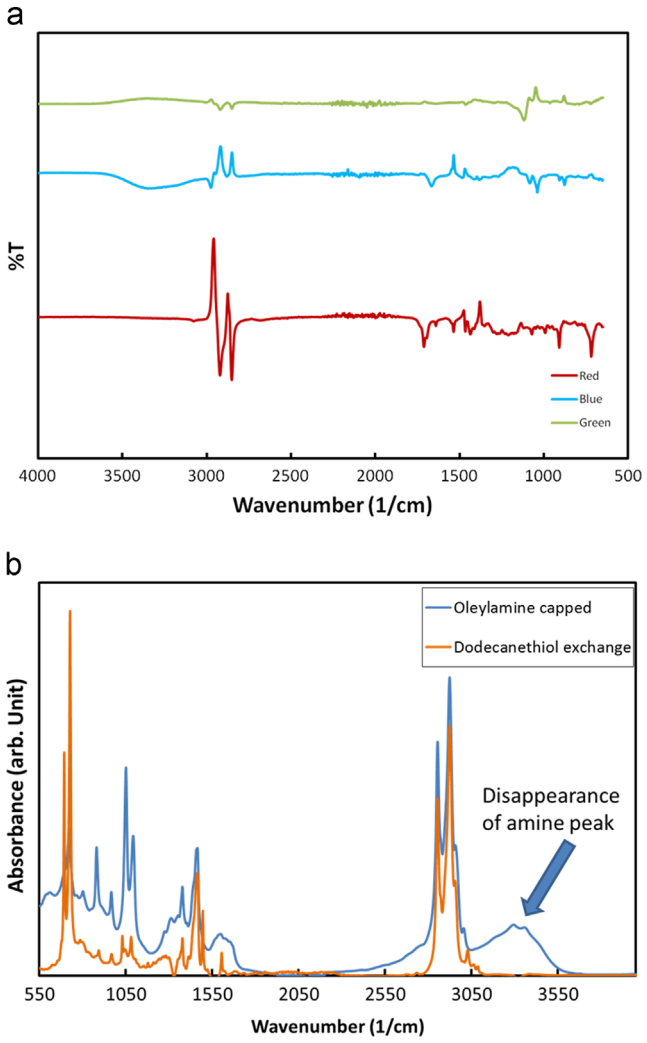

Fig. 9. (a): FTIR spectra of multicolored quantum dots. (b): FTIR Spectra of oleylamine capped and dodecanethiol exchanged non-stoichiometric kesterite nanocrystals.

3.8. Transmission electron microscopy

Fig. 10 shows TEM images of quantum dots of various samples. For sample 1, the TEM image (Fig. 10a) obtained from the lower portion of the layer shows a relatively big size crystal. Most of the crystals are rectangular and the sizes are in the range of ~30–25 nm. Whereas the small size fractions of nanocrystals are relatively small with size in the ~5–10 nm range (Fig. 10b). For sample 3, the small size fraction showing green luminescence was characterized. Most of the crystals are spherical shaped and the size is less than 5 nm. A corresponding FFT image is also shown in inset (See Fig. 10c). Such a

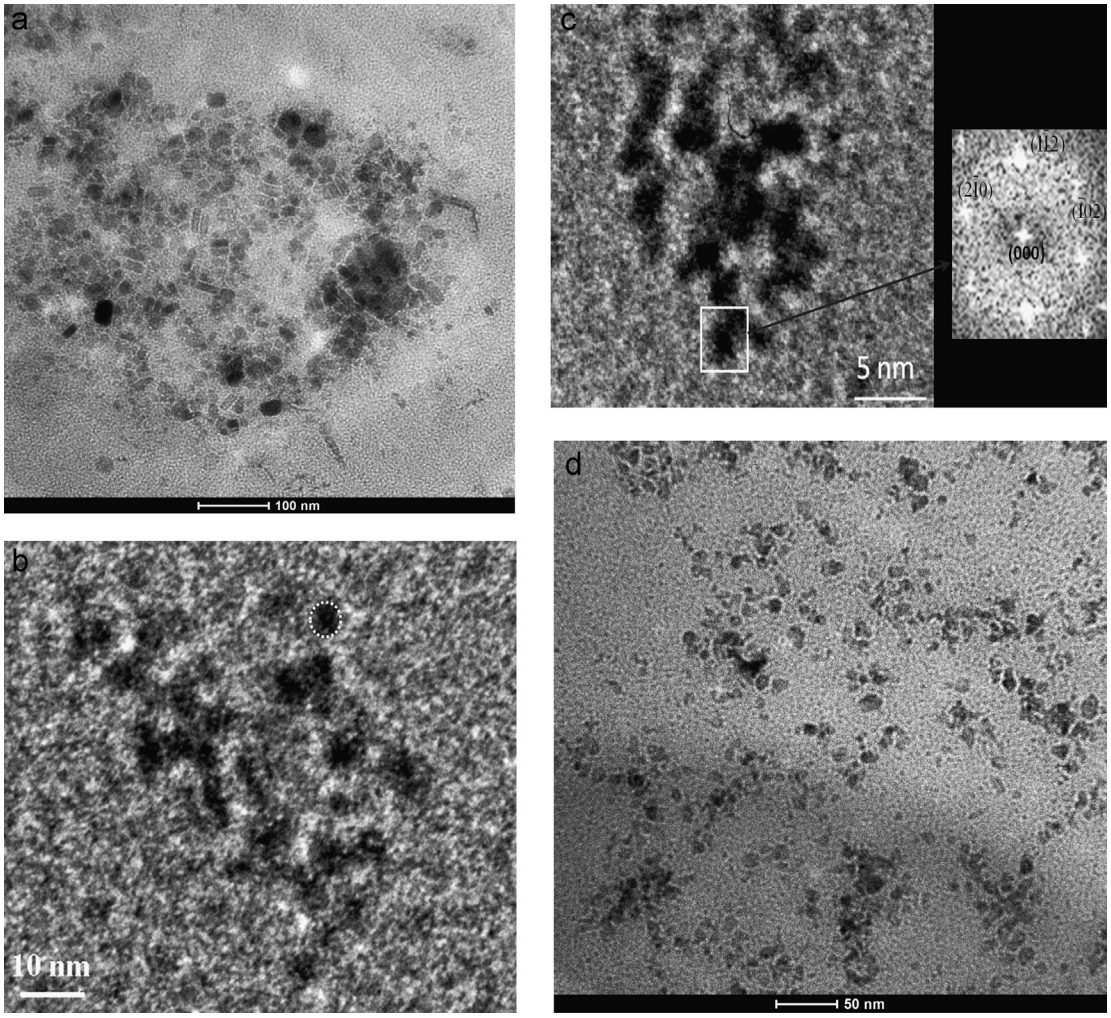

Fig. 10. TEM image of nanocrystals: (a) collected from sample 1, larger size fraction (b) collected from sample 1, smaller size fraction (c) collected from sample 3 (supernatant), FFT image is also shown in inset (d) collected from sample 2 (larger size fraction).

pattern indicates the formation of ZnS nanocrystals [34]. It also can be seen that many of the big crystals are agglomerated, small-sized crystals of dimensions less than 2 nm. Such small size nanocrystals are consistent with the large Raman line width observation. The size of the nanocrystals collected from larger size fraction (sample 2) was ~20 nm (See Fig. 10d). The morphology of these nanocrystals also depends on method of synthesis. It can be seen that for sample 2, most of the nanocrystals were spherical and relatively small in size.

3.9. Green -white light emitting diode

Fig. 11 shows images of epoxy hardener mixture with and without QDs. It can be seen that there is almost no luminescence for resin without quantum dots. However, a very good yellow-green luminescence can be seen for epoxy-hardener-QD paste. It also can be seen that our epoxy-hardener-QD resin turns into a paste (see tilted beaker) and finally into a solid when cured for longer duration. An effort was given to fabricate a light emitting diode using UV-LED. It can be seen that this LED is producing green light when power is turn on. It was observed that both photoluminescence spectra (original liquid and epoxy hardener) are not very different. Though luminance of our LED is not very high, it is fairly stable. An insignificant change in luminance was observed when LED was tested after 60 days of its fabrication. It is believed that QDs aggregation during epoxy-paste and afterwards causes scattering and re-absorption, which can cause deterioration in quantum yield. Hence such inefficiency should be addressed. We believe this research outcome can be a new domain for further investigation in order to produce an alternative methodology to get multicolor LEDs as well as next generation optical and plasmonic devices using non stoichiometric CZTS material [9,35].

4. Conclusions

In summary, by-product obtained during wet synthesis of colloidal Cu_2ZnSnS_4 nanocrystals was investigated for potential optical and biological applications. Most of the characterization results indicate that luminescent property of supernatant is due to the presence of quantum dots. It was observed that the

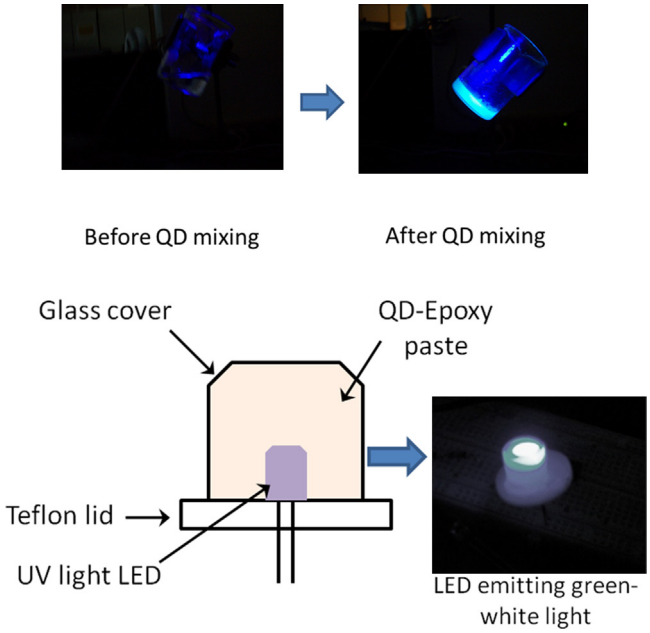

Fig. 11. Green light emitting diode synthesized using QD; epoxy-green gel is also shown for comparison. (For interpretation of the references to color in this figure legend, the reader is referred to the web version of this article.)

size of quantum dots was ~2–5 nm, which is aggregate of smaller non Cu_2ZnSnS_4 crystals whereas size of Cu_2ZnSnS_4 crystals was relative high. Our investigation indicates that these QDs are copper and tin doped ZnS nanocrystals where induced levels arise due to doping of these foreign elements during synthesis. Broad absorption spectra were shown by most of these quantum dots. These nanocrystals can be useful for various applications such as long duration display and general lighting because they are not likely to be photo-bleached. Luminescent resin was prepared using these quantum crystals and epoxy resin, which was further utilized for fabrication of green light emitting diode. Unlike conventional phosphors these LED will not suffer from unstable chemical properties. Ligand exchange was successfully conducted to remove most of the capping oleylamine using dodecanethiol. Such a process can useful, as it enables QDs to bind with various biological molecules and make them tunable for multiple medical applications.

Acknowledgments

Financial support from the University of Utah Research Foundation is thankfully acknowledged.

References

[1] V.I. Klimov, Semiconductor and Metal Nanocrystals, Synthesis and Electronic and Optical Properties, Marcel Dekker, Inc., New-York, 2004.
[2] N.i. Wei, T. Lu, F. Li, W. Zhang, B. Ma, Z. Lu, J. Qi, Transparent Ce: $Y_3Al_5O_{12}$ ceramic phosphors for white light-emitting diodes, Applied Physics Letters 101 (2012) 061902.
[3] Z. Xia, R.S. Liu, K.W. Huang, V. Drozd, $Ca_2Al_3O_6F:Eu^{2+}$: a green-emitting oxyfluoride phosphor for white light-emitting diodes, Journal of Materials Chemistry 22 (2012) 15183–15189.
[4] J. Tang, J. Chen, L. Hao, X. Xu, W. Xie, Q. Li, Green Eu^{2+}-doped $Ba_3Si_6O_{12}N_2$ phosphor for white light-emitting diodes: synthesis, characterization and theoretical simulation, Journal of Luminescence 131 (2011) 1101–1106.
[5] N. Hirosaki, R.J. Xie, K. Kimoto, T. Sekiguchi, Y. Yamamoto, T. Suehiro, M. Mitomo, Characterization and properties of green-emitting β-SiAlON: Eu^{2+} powder phosphors for white light-emitting diodes, Applied Physics Letters 86 (2005) 211905.
[6] H. Guo, H. Zhang, J. Li, F. Li, Blue–white–green tunable luminescence from $Ba_2Gd_2Si_4O_{13}:Ce^{3+},Tb^{3+}$ phosphors excited by ultraviolet light, Optics Express 18 (2010) 27257–27262.
[7] W.S. Song, J.H. Kim, J.H. Lee, H.S. Lee, Y.R. Do, H. Yang, Synthesis of color-tunable Cu–In–Ga–S solid solution quantum dots with high quantum yields for application to white light-emitting diodes, Journal of Materials Chemistry 22 (2012) 21901.
[8] W.S. Song, H. Yang, Fabrication of white light-emitting diodes based on solvothermally synthesized copper indium sulfide quantum dots as color converters, Applied Physics Letters 100 (2012) 183104.
[9] A.H. Ip, S.M. Thon, S. Hoogland, O. Voznyy, D. Zhitomirsky, R. Debnath, L. Levina, L.R. Rollny, G.H. Carey, A. Fischer, K.W. Kemp, I.J. Kramer, Z. Ning, A.J. Labelle, K.W. Chou, A. Amassian, E.H. Sargent, Hybrid passivated colloidal quantum dot solids, Nature Nanotechnology 7 (2012) 577–582.
[10] A. Khare, A.W. Wills, L.M. Ammerman, D.J. Norris, E.S. Aydil, Size control and quantum confinement in Cu_2ZnSnS_4 nanocrystals, Chemical Communications 47 (2011) 11721–11723.
[11] P.K. Sarswat, M.L. Free, An investigation of rapidly synthesized Cu_2ZnSnS_4 nanocrystals, Journal of Crystal Growth 372 (2013) 87–94.
[12] P.K. Sarswat, M.L. Free, A Comparative Study of Co-electrodeposited Cu_2ZnSnS_4 Absorber Material on fluorinated tin oxide and molybdenum substrates, Journal of Electronic Materials 41 (2012) 2210–2216.
[13] P.K. Sarswat, M.L. Free, Demonstration of a sol–gel synthesized bifacial CZTS photoelectrochemical cell, Physica Status Solidi A 208 (2011) 2861–2864.
[14] P.A. Fernandes, P.M.P. Salomé, A.F. da Cunha, Study of polycrystalline Cu_2ZnSnS_4 films by Raman scattering, Journal of Alloys and Compounds 509 (2011) 7600–7606.
[15] Y.C. Cheng, C.Q. Jin, F. Gao, X.L. Wu, W. Zhong, S.H. Li, Paul K. Chu, Raman scattering study of zinc blende and wurtzite ZnS, Journal of Applied Physics 106 (2009) 123505.
[16] X. Liu, X. Ni, J. Wang, X. Yu, A novel route to photoluminescent, water-soluble Mn-doped ZnS quantum dots via photopolymerization initiated by the quantum dots, Nanotechnology 19 (2008) 485602.
[17] W.G. Nilsen, Raman spectrum of cubic ZnS, Physical Review 182 (1969) 838–850.
[18] K.A. Alim, V.A. Fonoberov, M. Shamsa, A.A. Balandin, Micro-Raman investigation of optical phonons in ZnO nanocrystals, Journal of Applied Physics 97 (2005) 124313.
[19] Y. Zhao, H. Pan, Y. Lou, X. Qiu, J. Zhu, C. Burda, Plasmonic $Cu_{2-x}S$ nanocrystals: optical and structural properties of copper-deficient copper(I) sulfides, Journal of the American Chemical Society 131 (2009) 4253–4261.
[20] K. Manzoor, S. Johny, D. Thomas, S. Setua, D. Menon, S. Nair, Bio-conjugated luminescent quantum dots of doped ZnS: a cyto-friendly system for targeted cancer imaging, Nanotechnology 20 (2009) 065102.
[21] C. Persson, Electronic and optical properties of Cu_2ZnSnS_4 and $Cu_2ZnSnSe_4$, Journal of Applied Physics 107 (2010) 053710.
[22] P.Y. Yu, M. Cardona, Fundamentals of Semiconductors: Physics and Materials Properties, Springer, Heidelberg, 2010.
[23] R.N. Bhargava, D. Gallagher, Optical properties of manganese-doped nanocrystals of ZnS, Physical Review Letters 72 (1994) 416–419.
[24] A.A. Khosravi, M. Kundu, L. Jatwa, S.K. Deshpande, U.A. Bhagwat, M. Sastry, S.K. Kulkarni, Green luminescence from copper doped zinc sulphide quantum particles, Applied Physics Letters 67 (1995) 2702.
[25] F. Tan, S. Qu, J. Wu, K. Liu, S. Zhou, Z. Wang, Preparation of SnS_2 colloidal quantum dots and their application in organic/inorganic hybrid solar cells, Nanoscale Research Letters 6 (2011) 298.
[26] A.M. Brouwer, Standards for photoluminescence quantum yield measurements in solution, Pure and Applied Chemistry 83 (2011) 2213–2228.

[27] E. Talgorn, M.A. de Vries, L.D.A. Siebbeles, A.J. Houtepen, Photoconductivity enhancement in multilayers of CdSe and CdTe quantum dots, ACS Nano 5 (2011) 3552–3558.
[28] S. Hou, X. Zhang, H. Mao, J. Wang, Z. Zhu, W. Jing, Photoluminescence and XPS investigations of Cu^{2+}-doped ZnS quantum dots capped with polyvinylpyrrolidone, Solid State Physics B 246 (2009) 2333–2336.
[29] NIST X-ray Photoelectron Spectroscopy Database, Version 4.1 (National Institute of Standards and Technology, Gaithersburg, 2012); ⟨http://srdata.nist.gov/xps/⟩.
[30] Z. Mekhalif, L. Massi, F. Guittard, S. Geribaldi, J. Delhalle, X-Ray photoelectron spectroscopy study of polycrystalline zinc modified by n-dodecanethiol and 3-perfluorooctyl-propanethiol, Thin Solid Films 405 (2002) 186–193.
[31] G. Socrates, Infrared and Raman Characteristic Group Frequencies: Tables and Charts, John Wiley and Sons, England18.
[32] H. Gerung, S.D. Bunge, T.J. Boyle, C.J. Brinker, S.M. Han, Anhydrous solution synthesis of germanium nanocrystals from the germanium (II) precursor $Ge[N(SiMe_3)_2]_2$, Chemical Communications (2005) 1914–1916.
[33] B.K. Pong, B.L. Trout, J.Y. Lee, Modified ligand-exchange for efficient solubilization of cdse/zns quantum dots in water: a procedure guided by computational studies, Langmuir 24 (2008) 5270–5276.
[34] J. Cao, D. Han, B. Wang, L. Fan, H. Fu, M. Wei, B. Feng, X. Liu, J. Yang, Low temperature synthesis, photoluminescence, magnetic properties of the transition metal doped wurtzite ZnS nanowires, Journal of Solid State Chemistry 200 (2013) 317.
[35] G. Kumar, D.B. Singh, V.K. Tripathi, Surface enhanced Raman scattering of a surface plasma wave, Journal of Physics D: Applied Physics 39 (2006) 4436.